

Strain-induced phase selection in epitaxial Ge₂Sb₂Te₅ thin films

Mario Behrens ^{*}, Andriy Lotnyk [†], Jürgen W. Gerlach, and Bernd Rauschenbach 
 Leibniz Institute of Surface Engineering (IOM), Permoserstrasse 15, D-04318 Leipzig, Germany



(Received 8 August 2019; published 9 January 2020)

Controlling strain in hetero-epitaxial material systems can be used to optimize properties and functionalities for specific applications. For this purpose, a lattice mismatch between substrate and epitaxial layer is typically exploited. Beyond that, vicinal substrate surfaces can be used to enhance strain-induced effects. In both cases, a profound understanding of the impact of strain on the growth mode and the resulting structure and morphology of the epitaxial layer is of great importance in order to achieve the desired modifications. In this study, the impact of vicinal substrate surfaces on the phase, structure as well as on surface pattern formation in epitaxial phase-change material thin films is investigated. It is found that in the case of the prototypical phase-change material Ge₂Sb₂Te₅, the change from nominally flat Si(111) substrates to substrates with a miscut of 6° and terrace widths lying between 2 and 5 nm enhances compressive strain and a transition from 2D island nucleation to step-flow growth. This results in a different Ge₂Sb₂Te₅ phase evolution (change from metastable to stable phase) and surface nanostructuring by regularly arranged terraces that resemble the surface topography of the substrates. This work therefore provides deeper insights into different regimes of growth of epitaxial Ge₂Sb₂Te₅ thin films and paves the way for strain-induced modification possibilities such as band-gap tuning, optimization of the switching energy or the figure of merit.

DOI: [10.1103/PhysRevMaterials.4.015001](https://doi.org/10.1103/PhysRevMaterials.4.015001)

I. INTRODUCTION

In times of drastically growing digital data volumes, the development of novel storage technologies is of great importance [1]. A promising future nonvolatile data storage technology is phase-change memory technology [2,3]. This technology is based on the use of a phase-change material that exhibits a large contrast in electrical conductivity (up to five orders of magnitude) and optical reflectivity between its amorphous and crystalline phase [3,4]. This contrast is essential, since it allows for the encoding of information by setting the material in one of these two phases. The encoding process is realized by applying certain electrical or optical pulses. In particular, by applying a short and intense pulse, the material melts and subsequently quenches into the amorphous phase, whereas a longer and more moderate energy pulse results in the recrystallization of the material [5]. Advantageous for the application is the reversibility and the high speed of this switching process, which can be accomplished in less than a nanosecond [6]. Moreover, the phase-change memory technology shows excellent scaling capabilities [7]. The main disadvantages, however, are the high energy consumption, the limited data retention, and the substantial resistance drift [8]. Nevertheless, the phase-change memory technology is far from reaching its limits, and significant improvements can be expected in the future [9]. Currently, several studies explore the potential of epitaxial phase-change materials, as the advanced properties due to the high crystalline quality promise enhanced performance and novel device concepts

[10–17]. This approach thus aims to optimize devices via material optimization. Therefore, the control of the growth of epitaxial phase-change material thin films of application-relevant thicknesses below 100 nm is of great importance. The most prominent phase-change material is Ge₂Sb₂Te₅ (GST), which can exist in a thermodynamically stable trigonal phase (t-GST) and a metastable cubic phase (c-GST) [18,19]. In addition, the metastable phase of GST can possess a highly ordered configuration of intrinsic vacancies, where the vacancies accumulate into periodically spaced vacancy layers. Details on the epitaxy of these phases can be found in previous work, where in particular Si(111) has proven to be a suitable as well as technologically relevant substrate surface [13]. In recent studies, based on *in situ* RHEED observations, a layer-by-layer growth mode (Frank–van der Merwe mode) has been reported to occur during the epitaxy of GST thin films by PLD [20,21]. This growth mode is most likely favored by a relaxed growth of the thin films due to an almost strain-free van der Waals (vdW) epitaxy of the GST material on Si(111). An atomically resolved scanning transmission electron microscopy image of the Si(111)/GST interface can be found in Ref. [22]. As a result, the surfaces of the thin films are covered with 2D islands. In contrast, classical hetero-epitaxy is usually accompanied by a certain strain between the substrate and the epitaxial layer due to a certain lattice mismatch that favors the Volmer-Weber or Stransky-Krastanov growth mode resulting in energetically favored 3D islands, which relax the strain. This usually leads to a higher density of defects. The latter two growth modes are therefore undesirable when aiming to produce smooth and low-defect density layers. Nevertheless, it should be mentioned that strain up to some magnitude can be accommodated in the growing thin film without necessarily leading to defects

^{*}mario.behrens@iom-leipzig.de

[†]andriy.lotnyk@iom-leipzig.de

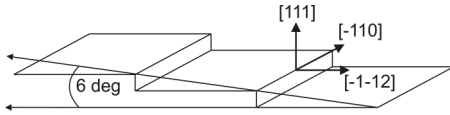


FIG. 1. Scheme of the surface of Si(111) substrate with a miscut of 6° .

[23]. Moreover, introducing strain into the vdW systems in a controlled manner offers possibilities to tune specific material properties and can therefore prove beneficial. In particular, strain effects due to the use of vicinal substrate surfaces as well as lattice mismatching in heterostructures have recently been discussed [24–28]. During the vdW epitaxy of GST, the Sb/Te surfactant atoms passivating the dangling bonds of the Si(111) substrate play a key role regarding the growth mode since they alter the diffusion barrier of the substrate, which influences the diffusion length of adatoms [29]. Moreover, the edge density of surface steps that represent favored exchange or nucleation sites plays another relevant role since it allows a special case of layer-by-layer growth called step-flow growth.

In summary, an advanced control of the epitaxy of GST thin films offers multifold engineering possibilities of thin film properties that could ultimately lead to enhanced device performances such as an increased programming window and reduced switching times [12,13,30]. Therefore, this study explores the effect of substrate surface terraces on the heteroepitaxial growth. In detail, the impact of the surface step density of the substrate on the phase and strain evolution as well as on the resulting growth mode during epitaxial growth of GST thin films on Si(111) substrates by pulsed laser deposition (PLD) is investigated.

II. EXPERIMENT

Epitaxial GST thin films of ~ 80 nm thickness were deposited by PLD using a KrF excimer laser of 248 nm wavelength and 20 ns pulse duration at a fluence of ~ 0.7 J cm $^{-2}$. The repetition rate was set to 2 Hz and a total of 4000 pulses were applied. The base pressure in the deposition chamber was 1.3×10^{-8} mbar. During the deposition, Ar was introduced resulting in a working pressure of 2.6×10^{-4} mbar. The GST thin films were grown on nominally flat Si(111) substrates ($\pm 0.5^\circ$ accuracy of surface orientation) and Si(111) substrates with a miscut of 6° along the $[-1-12]$ direction (see Fig. 1). Prior to deposition, the Si substrates were dipped into buffered HF acid for 30 s to remove the native oxide. During deposition, the substrate temperature was kept constant at 218° C. For laser ablation, a Ge $_2$ Sb $_2$ Te $_5$ compound target was used. The distance between target and substrate was set to 6 cm. After deposition, the GST thin films were capped by a thin LaAlO $_x$ (LAO) layer to prevent oxidation.

For structure analysis, x-ray diffraction (XRD) using Cu $K\alpha$ radiation was used. The diffractometer is equipped with a graphite monochromator. Note that a small proportion of $W-L_{\alpha 1/\alpha 2}$ radiation is transmitted by the monochromator and corresponding contributions are noticeable in the reciprocal space map measurements. In-plane pole figures were recorded using a 2.5° parallel slit collimator and a 2.5° parallel slit analyzer. The angular resolution in 2θ was 0.034° .

The deposition process is monitored *in situ* by reflection high energy electron diffraction (RHEED) using electrons of 30 keV and an incidence angle of $\sim 2^\circ$ with respect to the substrate surface.

The preparation of cross-sectional specimens for transmission electron microscopy (TEM) investigations was performed by a combination of focused gallium (30, 15, and 5 keV) and focused argon (900 and 500 eV) ion beam milling. The internal structure of GST thin films and the local structure between the substrates and thin films were observed in a probe Cs-corrected Titan 3 G2 60–300 microscope operating at 300 kV accelerating voltage. For scanning TEM (STEM), a probe-forming annular aperture of 20 mrad was used. Z contrast images were recorded with a high-angle annular dark-field (HAADF) STEM detector using annular ranges of 80–200 mrad while an annular-bright field (ABF) STEM covering annular ranges of 10–19 mrad was simultaneously used for acquisition of ABF-STEM images to take into account elastically Bragg scattered electrons.

III. RESULTS AND DISCUSSION

To explore the impact of the surface step density, epitaxial GST thin films are deposited on substrates with and without a miscut angle of 6° (using identical deposition parameters) and finally compared to each other. By using XRD methods, the structure and orientation of the as-deposited epitaxial GST thin films are characterized. Figure 2(a) depicts a θ - 2θ pattern

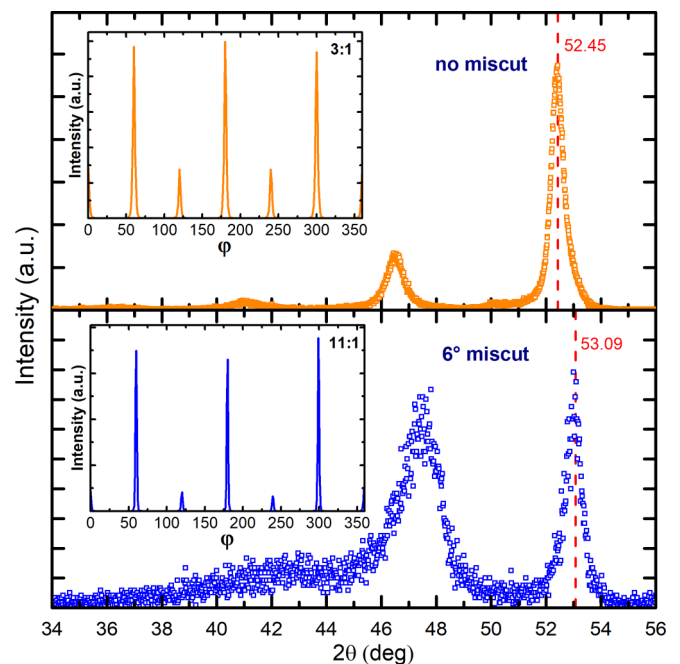


FIG. 2. XRD θ - 2θ patterns of as-deposited (a) epitaxial GST thin film deposited on substrate without a miscut and (b) epitaxial GST thin film deposited on substrate with a 6° miscut. Peak positions of metastable vacancy ordered Ge $_2$ Sb $_2$ Te $_5$ (vo-GST) and t-GST are indicated by red dashed lines. ϕ scans of t-GST{10-13} and c-GST{200} reflections indicating twinning behavior are shown in corresponding insets. Here, the ratios [3:1 in (a) and 11:1 in (b)] between the crystallite orientations are shown in the top right corner.

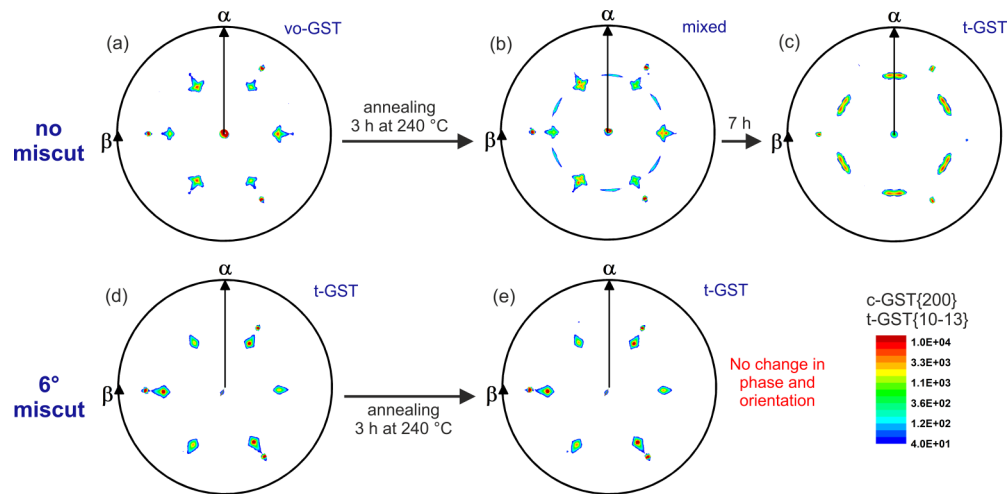


FIG. 3. In-plane XRD pole figure measurements of the $c\text{-GST}\{200\}$ and $t\text{-GST}\{10-13\}$ reflections, respectively. Pole figures of the as-deposited epitaxial GST thin films deposited on Si substrate without (a) and with (d) a miscut. (b,e) Corresponding pole figures after annealing at 240°C for 3 h. (c) Pole figure of the GST thin film deposited on the nominally flat substrate after annealing at 240°C for 7 h revealing complete transformation to $t\text{-GST}$. In the case of the thin film deposited on the miscut substrate, further annealing does not change the phase or the orientation.

of a GST thin film grown on a Si(111) substrate without a miscut (a nominally flat surface). For comparison, Fig. 2(b) shows the XRD pattern of a GST thin film deposited at the same parameters but on a substrate with a 6° miscut. Corresponding in-plane XRD pole figure measurements using the $\text{GST}\{200\}$ reflections are depicted in Figs. 3(a) and 3(c), respectively.

Clearly, the XRD results reveal high epitaxial quality, yet a remarkable difference is observed. In the case of a nominally flat substrate used, the deposition parameters result in the formation of epitaxial metastable vacancy ordered GST (vo-GST), whereas the thin film deposited on the substrate with a miscut of 6° grows in the stable trigonal phase of GST. This difference in phase evolution despite using the same deposition parameters becomes most evident at the XRD pattern in Fig. 2, where in (a) the peak positions of vo-GST and in (b) the peak positions of $t\text{-GST}$ reflections can be identified unambiguously. Consequently, an additional way to realize phase selectivity is found.

According to Fig. 3, the in-plane epitaxial relationships of the as-deposited $t\text{-GST}$ and vo-GST thin film are similar [$t\text{/vo-GST}\{0001\}||\text{Si}(111)$, $t\text{/vo-GST}\{01-10\}||\text{Si}[11-2]$] and the pole density maxima are situated at the same β values with respect to the pole density maxima coming from the substrate. Nevertheless, it should be noted that in Fig. 3(a) the pole density maxima are situated at a polar angle $\alpha = 55^\circ$, which corresponds to the tilt angle of the $t\text{-GST}\{10-13\}$ planes with respect to the substrate normal, whereas in Fig. 3(d) the pole density maxima can be found at a polar angle $\alpha = 57^\circ$, which corresponds to the tilt angle of the $c\text{-GST}\{200\}$ planes. This further confirms the different phase evolution found by the XRD pattern of Fig. 2.

It is also important to mention that the epitaxial in-plane relationship obeyed by the $t\text{-GST}$ structure grown on the miscut substrate has previously not been reported to the best of our knowledge. Even with subsequent annealing at 240°C for several hours, the orientation of the as-deposited $t\text{-GST}$

thin films does not change [see Fig. 3(e)], whereas in the case of the vo-GST thin film deposited on the substrate without a miscut, the orientation changes as the vo-GST slowly transforms into $t\text{-GST}$ [see Figs. 3(b) and 3(c)]. This transformation becomes apparent by the additional appearance of pole density maxima corresponding to $t\text{-GST}\{10-13\}$ reflections as previously reported in the literature (epitaxial relationship: [$t\text{-GST}(0001)||\text{Si}(111)$, $t\text{-GST}[11-20]||\text{Si}[11-2]$]) [13,21]. During this transformation, the preferred epitaxial orientation is achieved, as the change in orientation [Figs. 3(a)–3(c)] reduces the misfit between the substrate and the epitaxial GST layer from $+9.6\%$ [in the case of the orientation relationship shown in Fig. 3(e)] to -4.8% [in the case of the orientation relationship shown in Fig. 3(c)]. The larger misfit value for $t\text{-GST}$ grown on the miscut substrate points out the accumulation of higher residual strain (see below) during the thin film growth compared to the thin films deposited on the nominal flat surfaces. In the case when the miscut substrate is used, however, the structural rearrangement is constrained.

Apart from the impact on the phase formation and the epitaxial in-plane relationship, the use of a miscut substrate further changes the degree of twinning. In epitaxial GST thin films grown on Si(111), the presence of 180° rotational twin domains is regularly observed, where one of the crystallite orientations is usually dominant with a ratio between the two orientations of about 3:1 [21,31]. This ratio is also valid for the epitaxial vo-GST thin films fabricated in this work, which can be seen in the φ scan of the $\text{GST}\{200\}$ reflections shown in Fig. 2(a). However, when using a miscut substrate, one of the orientations becomes significantly dominant with a ratio of 11:1 [see the corresponding φ scan in Fig. 2(b)].

Consequently, a substantial change in the growth process can be expected [e.g., by (i) a change of phase, (ii) a constraint of structural rearrangement, (iii) suppression of twinning, (iv) step formation at the surface, and (v) accumulation of strain (see below)] when using the 6° miscut substrate. In

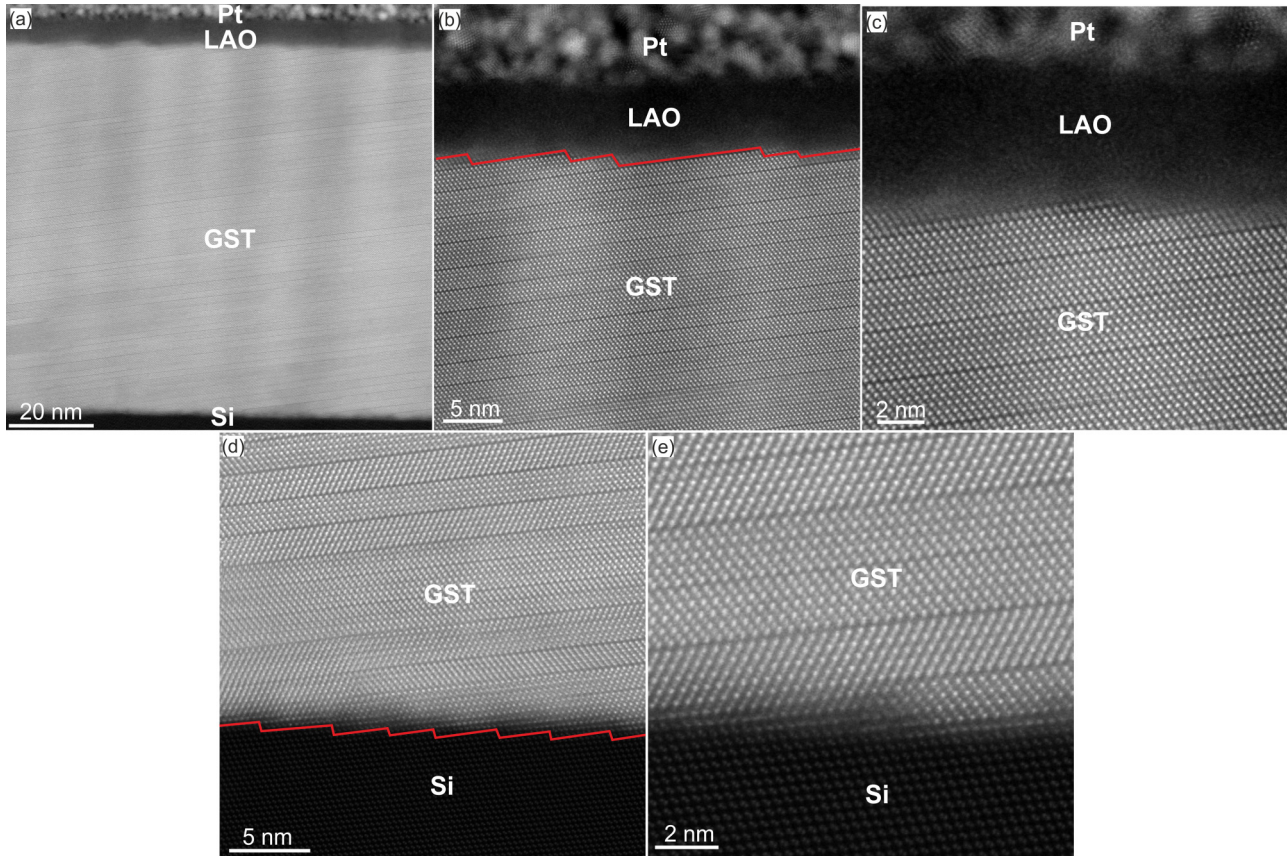


FIG. 4. HAADF-STEM images of an epitaxial t-GST thin film deposited on Si(111) with a 6° miscut. The GST surface is nanostructured by steps and terraces (b), (c). The step height and the terrace width at the GST thin film surface are slightly larger than those of the Si substrate due to the miscut (d), (e).

particular, it is assumed that the regularly spaced step edges of the miscut substrate cause a transition from the 2D growth to the step-flow growth regime, where adatoms first diffuse to the step edges before they nucleate [32]. That in turn reduces twinning, which is usually favored by random nucleation of 2D domains on the terraces.

Further support for the presence of step-flow growth is found by STEM studies of the thin GST films.

Figure 4 shows STEM images of the GST thin film deposited on Si(111) substrate with a 6° miscut. The images confirm the presence of t-GST. Importantly, at the surface of the thin film [Figs. 4(b) and 4(c)], periodically arranged terraces with a width of around 2–10 nm are found. These terraces possess a width up to twice as large as the terraces of the substrate [see Figs. 4(d) and 4(e)] and indicate that step bunching (usually attributed to the growth of larger terraces and an increased surface roughness) occurs during the step-flow growth process.

At this point, it is important to mention that a prerequisite for step-flow growth is that the diffusion length of the adatoms is at least in the range of the terrace width of the substrate and that each layer must be completed before the formation of an overlying layer begins. Here, the incoming flux F of incoming species as well as the diffusion constant D are crucial quantities. Depending on the laser intensity and the repetition rate during the PLD process, the flux can adopt

a quasicontinuous as well as a pulsed character resulting in different regimes of growth leading to different island densities. In the case of a continuous flux where the intensity allows the adatoms to unfold their full mobility before they nucleate, the average island density depends on $(D/F)^\gamma$ with $\gamma = 0.17$ [33,34]. In this work, however, a chopped flux is used, where all adatoms are incorporated into the structure before the next pulse of material arrives at the substrate. In detail, a pulse repetition rate of 2 Hz was used to deposit the 80-nm-thick thin film by applying a total of 4000 pulses. Accordingly, each pulse deposits roughly 0.02 nm of GST resulting in an effective flux of 0.2 monolayers per second. In Fig. 5, the temporal evolution of the RHEED specular spot intensity during epitaxial growth of GST thin films on nominally flat Si(111) substrates after application of a single deposition pulse at $t = 0$ s is shown. It can be observed that directly after the pulse, the RHEED intensity decreases due to the deposited species first increasing the step density on the already deposited GST layers and thus enhancing diffuse scattering of electrons. However, during a certain time period the adatoms diffuse to their nucleation sites and attach to existing layers, which leads to a recovery of the RHEED intensity. This implies that single atomic layers form, where the adatoms gradually complete the layers by attaching to their edges. The question about the composition of these layers during formation, however, is difficult to answer since vo/t-GST

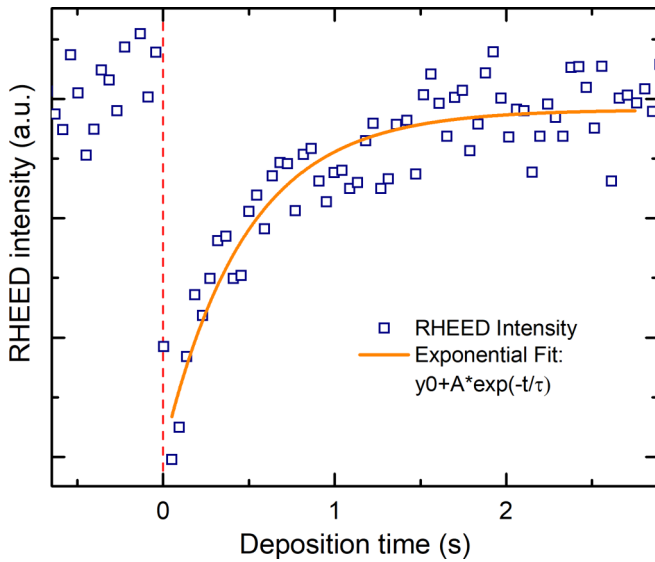


FIG. 5. RHEED intensity relaxation. Single deposition pulse applied at $t = 0$ s (red dashed line). Exponential fit to data provides a mean lifetime $\tau = 0.48$ s of an adatom.

exhibit a certain degree of compositional randomness on their cation layers (Ge/Sb/vacancy layers). However, at the latest when a complete unit cell is formed, a partially ordered stacking sequence should be established, according to the literature [18,35,36]. This partially ordered stacking sequence could be realized directly during deposition of the individual layers or by interlayer diffusion after deposition of multiple layers (note that the substrate is heated during deposition).

By exponential fitting of the recovery of the RHEED intensity, the mean lifetime $\tau = 0.48$ s of an adatom before incorporation into the lattice is obtained. Together with the diffusion constant, this finally allows us to determine the diffusion length of the adatoms ($L = \sqrt{D\tau}$). In the case of Ge, Sb, or Te diffusion on GST at 600 K, a maximum diffusion length of approximately 2×10^{-5} m is calculated, which considerably exceeds the terrace width of the miscut Si(111) substrate and thus would support step-flow growth. Moreover, assuming a terrace width of 5 nm, the lifetime of an adatom on such a terrace until incorporation would be around $0.1 \mu\text{s}$ and hence short enough to exclude multiple depositions on top of the still forming layers due to successive pulses [33,37,38].

Interestingly, besides a nanostructured surface, the STEM images further reveal areas of disordered GST structure close to the step edges of the substrate. These areas are indicated by the orange arrows in Figs. 6(a) and 6(b), where the interface between the substrate and the thin film can be seen in more detail. According to the step-flow growth mode, the GST layers start forming at the step edges followed by quasi-van der Waals epitaxial growth across the terrace. Hence, considering only an isolated terrace, the GST layer forms almost strain-free despite the misfit between the lattice constants of the film and the substrate (a_{film} and a_{sub}). However, when the complete terrace is finally covered, a residual space Δd between the GST lattice and the terrace width can occur [see the scheme in Fig. 6(c)], which results from the mismatch

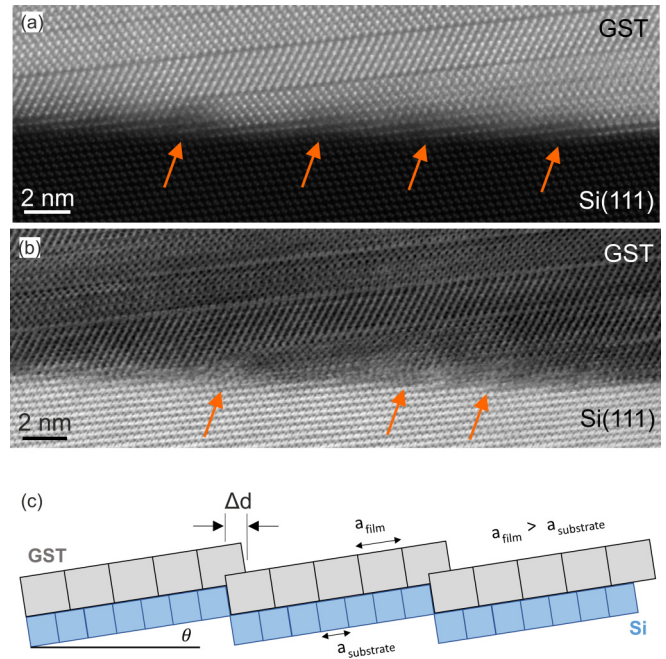


FIG. 6. (a) HAADF-STEM image and (b) ABF STEM image of the interface between Si(111) substrate with a miscut $\theta = 6^\circ$ and GST thin film. Disordered regions at substrate steps are indicated by orange arrows. (c) Scheme of strain generation at the Si/GST interface. Alignment of GST lattice results in strained terraces.

between the width of the terrace and the integer number of unit cells of GST that such a terrace could accommodate [39,40]. To align with the layers of the adjacent terraces, the layers must be compressed or stretched by the overlap Δd , which finally leads to the strained growth of the thin film. Note that the vertical mismatch at the step edge can additionally contribute to the accumulation of strain in the GST thin film.

Therefore, in order to investigate the presence of strain in the GST thin film grown on the miscut substrate, XRD reciprocal space maps are recorded.

In Fig. 7, reciprocal space maps spanning the GST(10-13) and Si(224) reflections of epitaxial GST thin films deposited on Si(111) substrates with and without miscut are shown. It is observed that the degree of peak broadening of the GST(10-13) reflections attributed to the mosaic spread is approximately the same in both cases. In the case when the GST thin film is grown on the substrate without a miscut [Fig. 7(a)], the thin film is relaxed and the reflections are roughly lying on the relaxation line going through the origin. However, in the case when a miscut substrate is used [Fig. 7(b)], the GST(10-13) reflection position is shifted along the Q_x direction (parallel to the [-1-12] direction) toward the position of the Si(224) peak, which indicates an in-plane compression of the GST lattice. Consequently, the GST thin film is compressively strained due to a residual space Δd between the terrace width of the substrate and a multiple of the in-plane lattice constant of GST. Interestingly, Zallo *et al.* reported that the deposition of epitaxial Ge-Sb-Te on Si(111) with a miscut of 3° – 6° by molecular beam epitaxy also favors the formation of the thermodynamically stable phase [24]. However, in their work, no clear discrimination between the vacancy ordered metastable

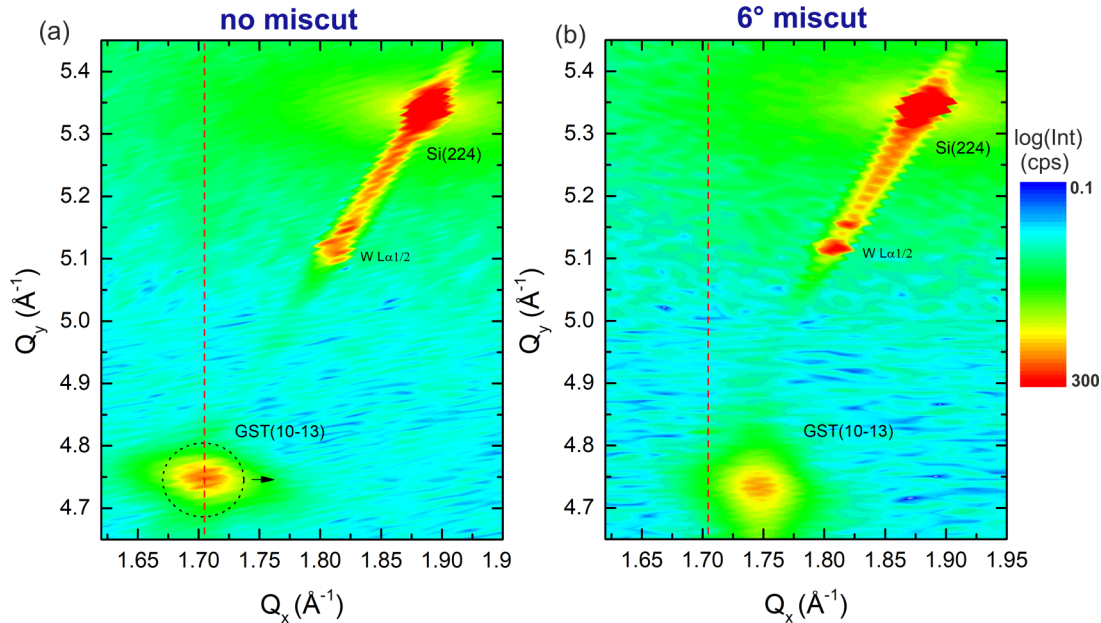


FIG. 7. XRD reciprocal space maps in the range of the Si(224) and GST(10-13) diffraction peaks of an epitaxial GST thin film deposited on substrate with and without a 6° miscut. Shift of GST(10-13) diffraction peak along Q_x indicated by a black arrow.

and the stable phase of Ge-Sb-Te is made. They propose that Ge-Sb-Te grows constrained on both sides of a terrace due to the Si steps, which leads to strong coupling at the step edges. This allows us to modulate the growth of GST from purely vdW epitaxy to a combination of classical and vdW epitaxy. In the present work, the strained epitaxial growth of GST on miscut Si(111) is confirmed (although a different deposition method is used) and the underlying growth mode is additionally revealed. Besides that, it is suggested that instead of a combination of classical and vdW epitaxy, mainly the vdW epitaxy is present and the modifications of thin film properties originate from surface-step-terrace-induced strain.

In summary, the presented results demonstrate that when using a substrate with a 6° miscut, the thermodynamically stable phase of GST (t-GST) can be grown epitaxially using deposition parameters resulting in the metastable vo-GST phase on nominally flat substrates (i.e., less energy is required). Besides that, in the resulting thin film, structural rearrangement is constrained and twinning largely reduced. These aspects could prove beneficial for the application since the high-quality layered structure of t-GST provides a higher reflectivity and conductivity contrast with respect to the amorphous phase and enables layer-switching processes that offer potential for novel storage concepts [41–44].

IV. CONCLUSION

In conclusion, an increased surface step density of the substrate causes substantial changes in the growth process during the epitaxy of GST thin films, leading to a gain in energy that enables the formation of the thermodynamically stable GST phase at conditions resulting usually in the formation of the metastable vo-GST phase. Moreover, twinning is reduced and the in-plane orientation constrained. Evidence is found that step-flow growth is the dominant growth mode leading to a nanostructured surface. Generally, the mismatch between the film unit cell arrangement and the substrate surface-step-terrace dimensions will result in an additional strain energy that cannot be released via dislocations and will be stored in the heteroepitaxial films. As the GST thin film continues to grow, residual matching-induced strain energy will accumulate in the film and can significantly alter its microstructure and thus its physical and electrical properties.

ACKNOWLEDGMENTS

The financial support of the Free State of Saxony within the project “Switching with light” is kindly acknowledged. The authors thank A. Mill and H. Bryja for TEM specimen preparation and M. Mensing for fruitful discussions.

- [1] D. Reinsel, J. Gantz, and J. Rydning, *IDC White Paper* (International Data Corporation, Framingham US, 2018).
- [2] M. Wuttig and N. Yamada, *Nat. Mater.* **6**, 824 (2007).
- [3] I. Friedrich, V. Weidenhof, W. Njoroge, P. Franz, and M. Wuttig, *J. Appl. Phys.* **87**, 4130 (2000).
- [4] M. Wuttig, *Nat. Mater.* **4**, 265 (2005).
- [5] S. Raoux, in *Annual Review of Materials Research* (Annual Reviews, Palo Alto, 2009), p. 25.

- [6] F. Rao *et al.*, *Science* **358**, 1423 (2017).
- [7] R. E. Simpson, M. Krbal, P. Fons, A. V. Kolobov, J. Tominaga, T. Uruga, and H. Tanida, *Nano Lett.* **10**, 414 (2010).
- [8] P. Noé, C. Vallée, F. Hippert, F. Fillot, and J.-Y. Raty, *Semicond. Sci. Technol.* **33**, 013002 (2017).
- [9] W. Zhang, R. Mazzarello, M. Wuttig, and E. Ma, *Nat. Rev. Mater.* **4**, 150 (2019).

- [10] W. Braun, R. Shayduk, T. Flissikowski, M. Ramsteiner, H. T. Grahn, H. Riechert, P. Fons, and A. Kolobov, *Appl. Phys. Lett.* **94**, 041902 (2009).
- [11] E. Thelander, J. W. Gerlach, U. Ross, F. Frost, and B. Rauschenbach, *J. Appl. Phys.* **115**, 213504 (2014).
- [12] V. Bragaglia, F. Arciprete, W. Zhang, A. M. Mio, E. Zallo, K. Perumal, A. Giussani, S. Cecchi, J. E. Boschker, H. Riechert, S. Privitera, E. Rimini, R. Mazzarello, and R. Calarco, *Sci. Rep.* **6**, 23843 (2016).
- [13] M. Behrens, A. Lotnyk, Ro, J. Griebel, P. Schumacher, J. W. Gerlach, and B. Rauschenbach, *Crystengcomm.* **20**, 3688 (2018).
- [14] M. Behrens, A. Lotnyk, J. W. Gerlach, I. Hilmi, T. Abel, P. Lorenz, and B. Rauschenbach, *Nanoscale* **10**, 22946 (2018).
- [15] M. M. Dück, T. Schäfer, S. Jakobs, C.-F. Schön, H. Niehaus, O. Cojocar-Miréidin, and M. Wuttig, *Phys. Status Solidi (RRL)* **13**, 1800578 (2019).
- [16] J. Momand, R. Wang, J. E. Boschker, M. A. Verheijen, R. Calarco, and B. J. Kooi, *Nanoscale* **9**, 8774 (2017).
- [17] R. E. Simpson, P. Fons, A. V. Kolobov, T. Fukaya, M. Krbal, T. Yagi, and J. Tominaga, *Nat. Nanotechnol.* **6**, 501 (2011).
- [18] B. J. Kooi and J. T. M. De Hosson, *J. Appl. Phys.* **92**, 3584 (2002).
- [19] T. Matsunaga, N. Yamada, and Y. Kubota, *Acta Crystallogr. Sect. B* **60**, 685 (2004).
- [20] I. Hilmi, A. Lotnyk, J. W. Gerlach, P. Schumacher, and B. Rauschenbach, *Mater. Des.* **115**, 138 (2017).
- [21] I. Hilmi, A. Lotnyk, J. W. Gerlach, P. Schumacher, and B. Rauschenbach, *Mater. Des.* **168**, 107657 (2019).
- [22] A. Lotnyk, M. Behrens, and B. Rauschenbach, *Nanoscale Adv.* **1**, 3836 (2019).
- [23] U. Ross, A. Lotnyk, E. Thelander, and B. Rauschenbach, *J. Alloys Compd.* **676**, 582 (2016).
- [24] E. Zallo, S. Cecchi, J. E. Boschker, A. M. Mio, F. Arciprete, S. Privitera, and R. Calarco, *Sci. Rep.* **7**, 1466 (2017).
- [25] R. Wang, F. R. L. Lange, S. Cecchi, M. Hanke, M. Wuttig, and R. Calarco, *Adv. Funct. Mater.* **28**, 1705901 (2018).
- [26] M. N. Schneider, P. Urban, A. Leineweber, M. Doblinger, and O. Oeckler, *Phys. Rev. B* **81**, 184102 (2010).
- [27] J. Kalikka, X. Zhou, E. Dilcher, S. Wall, J. Li, and R. E. Simpson, *Nat. Commun.* **7**, 11983 (2016).
- [28] P. A. Vermeulen, J. Mulder, J. Momand, and B. J. Kooi, *Nanoscale* **10**, 1474 (2018).
- [29] D. Kandel and E. Kaxiras, *Phys. Rev. Lett.* **75**, 2742 (1995).
- [30] M. Behrens, A. Lotnyk, J. W. Gerlach, M. Ehrhardt, P. Lorenz, and B. Rauschenbach, *ACS Appl. Mater. Interfaces* **11**, 41544 (2019).
- [31] E. Thelander, J. W. Gerlach, U. Ross, A. Lotnyk, and B. Rauschenbach, *Appl. Phys. Lett.* **105**, 221908 (2014).
- [32] M. Lippmaa, N. Nakagawa, M. Kawasaki, S. Ohashi, and H. Koinuma, *Appl. Phys. Lett.* **76**, 2439 (2000).
- [33] B. Hinnemann, H. Hinrichsen, and D. E. Wolf, *Phys. Rev. E* **67**, 011602 (2003).
- [34] J. Villain, A. Pimpinelli, L. Tang, and D. Wolf, *J. Phys. I* **2**, 2107 (1992).
- [35] A. Lotnyk, U. Ross, S. Bernutz, E. Thelander, and B. Rauschenbach, *Sci. Rep.* **6**, 26724 (2016).
- [36] Y. Zheng, Y. Wang, T. Xin, Y. Cheng, R. Huang, P. Liu, M. Luo, Z. Zhang, S. Lv, Z. Song, and S. Feng, *Commun. Chem.* **2**, 13 (2019).
- [37] L. Guan, D. Zhang, X. Li, and Z. Li, *Nucl. Instrum. Methods Phys. Res. Sect. B* **266**, 57 (2008).
- [38] T. Li *et al.*, *J. Phys. Chem. C* **123**, 13377 (2019).
- [39] H. Lu, C. Zhang, H. Guo, H. Gao, M. Liu, J. Liu, G. Collins, and C. Chen, *ACS Appl. Mater. Interfaces* **2**, 2496 (2010).
- [40] G. Yao, M. Gao, Y. Ji, W. Liang, L. Gao, S. Zheng, Y. Wang, B. Pang, Y. B. Chen, H. Zeng, H. Li, Z. Wang, J. Liu, C. Chen, and Y. Lin, *Sci Rep* **6**, 34683 (2016).
- [41] A. Lotnyk, T. Dankwort, I. Hilmi, L. Kienle, and B. Rauschenbach, *Scr. Mater.* **166**, 154 (2019).
- [42] A. V. Kolobov, P. Fons, Y. Saito, and J. Tominaga, *ACS Omega* **2**, 6223 (2017).
- [43] J.-J. Wang, J. Wang, H. Du, L. Lu, P. C. Schmitz, J. Reindl, A. M. Mio, C.-L. Jia, E. Ma, R. Mazzarello, M. Wuttig, and W. Zhang, *Chem. Mater.* **30**, 4770 (2018).
- [44] J.-J. Wang, J. Wang, Y. Xu, T. Xin, Z. Song, M. Pohlmann, M. Kaminski, L. Lu, H. Du, C.-L. Jia, R. Mazzarello, M. Wuttig, and W. Zhang, *Phys. Status Solidi (RRL)* **13**, 1900320 (2019).